CHEMISTRY
AN ASIAN JOURNAL

DOI: 10.1002/asia.200800151

Photophysical and Duplex-DNA-Binding Properties of Distamycin Dimers Based on 4,4′- and 2,2′-Dialkoxyazobenzenes as the Core

Sumana Ghosh,[a] Dandamudi Usharani,[b] Susmita De,[b] Eluvathingal D. Jemmis,[b] and Santanu Bhattacharya*[a, c]

Abstract: Distamycin-based tetrapeptide (**1**) was covalently tethered to both ends of the central dihydroxyazobenzene moiety at either the 2,2′ or 4,4′ positions. This afforded two isomeric, distamycin–azobenzene–distamycin systems, **2** (*para*) and **3** (*ortho*), both of them being photoisomerizable. Illumination of these conjugates in solution at approximately 360 nm induced photoisomerization and the time course of the process was followed by UV/Vis and ^{1}H NMR spectroscopy. The kinetics of the thermal reversion at various temperatures of *cis* to *trans* isomers of the conjugates obtained after photoillumination were also examined. This afforded the respective thermal-activation parameters. Both the molecular architecture and the location of the substituent around the core azobenzene determined the rate and activation-energy barrier for the *cis*-to-*trans* back-isomerization of these conjugates in solution. Duplex–DNA binding of the conjugates and the changes in DNA-binding efficiency upon photoisomerization was also examined by CD spectroscopy, thermal denaturation studies, and a Hoechst displacement assay. The conjugate **2** showed higher DNA-binding affinity and a greater change in the DNA-binding efficiency upon photoisomerization compared with its 2,2′-disubstituted counterpart. The experimental findings were substantiated by using molecular-docking studies involving each conjugate with a model duplex d[(GC(AT)$_{10}$CG)]$_2$ DNA molecule.

Keywords: azo compounds · DNA structures · minor groove binders · peptides · photochemistry

Introduction

The azobenzene group is known to undergo *cis*-to-*trans* photoisomerization reversibly upon UV/Vis photoillumination.[1] Such light-induced isomerization of azobenzene is accompanied by significant changes in geometry and polarity of the chromophore.[2] The unique properties of this moiety has been utilized by introducing it both in the side chain and at the backbone of peptide, proteins, oligonucleotides, and phospholipids, so that light-induced photoisomerization leads to significant changes in the properties of such biomolecules.[3–7] Recently, attention has been focused on achieving artificial control of gene expression because of its potential applications in cell biology and pharmacology. Thus, an azobenzene group has been tethered into many transcription factors to convert them from a non-DNA-binding protein to an active form. The resulting conjugates are capable of recognizing the appropriate binding sites at the promoter region in the presence of light.[8,9] Furthermore, azobenzene has also been appended at various positions of the T7-pro-

[a] S. Ghosh, S. Bhattacharya
Department of Organic Chemistry
Indian Institute of Science
Bangalore 560 012 (India)
Fax: (+91) 80-2360-0529
E-mail: sb@orgchem.iisc.ernet.in

[b] D. Usharani, S. De, E. D. Jemmis[+]
Department of Inorganic and Physical Chemistry
Indian Institute of Science
Bangalore 560 012 (India)

[c] S. Bhattacharya
Chemical Biology Unit
Jawaharlal Nehru Centre of Advanced Scientific Research
Bangalore 560 012 (India)

[+] Current address:
Indian Institute of Science Education and Research
Thiruvananthapuram, CET Campus
TVM 695 016, Kerala (India)

Supporting information for this article is available on the WWW under http://dx.doi.org/10.1002/asia.200800151.

moter site to modulate the transcription machinery in the presence or absence of light.[10]

Distamycin has been a good choice for the design of DNA-minor-groove-binding small molecules as it has potential to permeate across human cells and could participate in regulation of transcription of specific genes.[11] Owing to our interest in the design of DNA-binding/cleaving systems,[12] earlier we examined in detail the AT-sequence-specific DNA-recognition properties of a number of synthetic distamycin analogues including its tail-to-tail dimers.[13,14] We also reported the synthesis and characterization of distamycin-linked oligodeoxynucleotides.[15] We have now developed photoisomerizable DNA-binding molecular entities based on distamycin. Accordingly, we have synthesized conjugates by appending two distamycin arms at both ends of two isomeric dihydroxyazobenzene moieties. The azobenzene core might be compatible with the minor groove of DNA, as such loci are known to accommodate hydrophobic aromatic rings.[16] Herein, we report the synthesis of two azobenzene distamycin conjugates **2** and **3** (Scheme 1) that bear tetra *N*-methylpyrrole-based polyamide groups at the 2,2′- and 4,4′-positions of the dialkoxyazobenzene core. Each distamycin arm has been connected to the azobenzene core through an *N*-methyldiethylenetriamine linkage. This feature ensures protonation in solution at both ends of the azobenzene core at the C termini of the distamycin oligopeptide arms at physiological pH values. With the compounds **2** and **3** in hand, we sought to know whether there is any influence on the rate of azobenzene isomerization in solution while the oligopeptide arm is connected through the *ortho* (2,2′) or *para* (4,4′) positions of the core azobenzene. We were also interested to know how incorporation of an azobenzene moiety in conjugates **2** and **3** interferes with the distamycin binding on duplex-DNA minor grooves. Finally, it was of interest to see how photoisomerization of distamycin–azobenzene conjugates alters their duplex-DNA binding.

To address the above issues, we first examined the photoisomerization of ligands **2** and **3** in dimethylsulfoxide (DMSO) solution by irradiating them at a wavelength of approximately 360 nm. This was followed by both UV/Vis spectroscopy and ^{1}H NMR analyses. Poly [d(AT)]·poly [d(TA)] DNA-binding abilities of individual conjugates and the changes in DNA-binding efficiency during the photoisomerization process were studied by CD spectroscopy, thermal denaturation studies, and a Hoechst displacement assay. We have also compared the DNA-binding affinity of different photoirradiated forms of **2** and **3** with that of the parent distamycin **1**. Ligand **2** showed higher DNA-binding affinity and induced a greater change in the duplex-DNA binding upon photoisomerization compared with its *ortho–ortho* disubstituted counterpart, **3**. To understand the basis by which the interactions of such conjugates are governed on the duplex DNA, molecular docking by using duplex d[(GC(AT)$_{10}$CG)]$_2$ DNA as a model scaffold was performed. Both experimental and theoretical studies demonstrate that DNA-binding characteristics of such new azobenzene–distamycin conjugates are remarkably dependent on the position of the connectivity between the azobenzene and the oligopeptide units.

Results and Discussion

Structural Features of Conjugates

All the bis-alkoxy-substituted azobenzene distamycin conjugates (**2**, **3**) and parent distamycin **1** were minimized at the HF/3-21G level of theory by using the Gaussian 03[17] program. The total energies and relative energies of the *cis* and *trans* forms of these structures have been recorded in Table 1. These calculations indicate that the linker length between the azobenzene and distamycin arm in **2** and **3** ranges from 10.7–11 Å. Moreover the distance around the azobenzene moiety (XPhN=NPhX) (X = $-OCH_2-$) changes from approximately 11.8 Å to approximately 8.3 Å in the case of **2** and approximately 6.5 Å to approximately 5.4 Å in the case of **3** during *trans* to *cis* isomerization. The calculated energy difference between the *trans* and *cis* forms of **2** is approximately 13.12 kcal mol^{-1}, whereas that for **3** is approximately

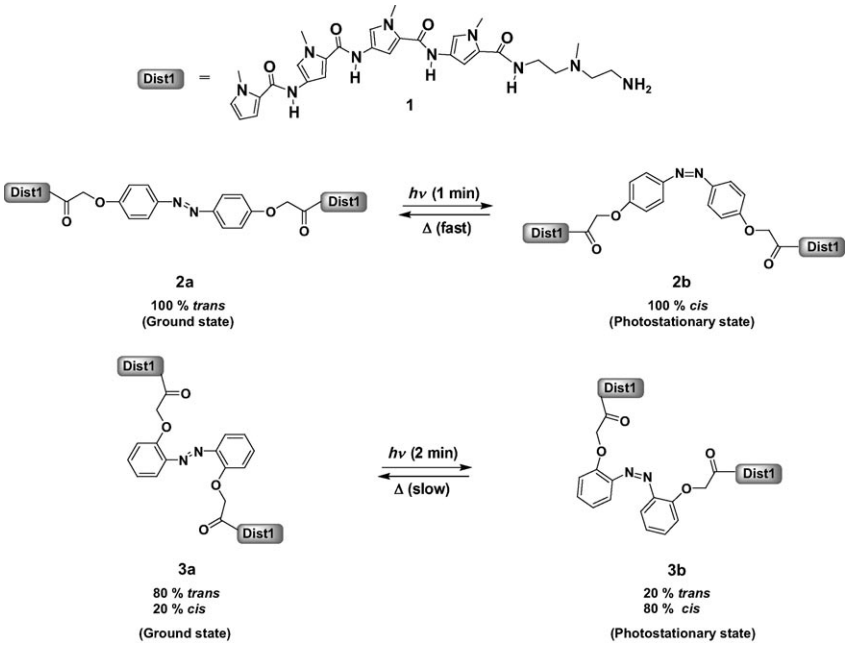

Scheme 1. Schematic representation of the effect of photo-illumination and thermal reversal of 4,4′-di-alkoxy-azobenzene distamycin derivatives **2** and 2,2′-di-alkoxyazobenzene distamycin derivatives **3**.

Table 1. The total and relative energies of Gaussian (HF/3-21G)-optimized **1** and the *cis* and *trans* forms of the ligands **2** and **3**, the distance around the azobenzene (XPhN=NPhX) (X = $-OCH_2-$), and the length along the linker with azobenzene moiety [$-(CH_2)_2NMe(CH_2)_2NHYPhN=NPhYNH(CH_2)_2NMe(CH_2)_2-$] (Y = $-OCH_2CO$) for both isomeric forms of the azobenzene–distamycin conjugates.

Ligand	Total energy [a.u.]	Relative energy [kcal mol^{-1}]	Distance around azobenzene, azobenzene-linker distance [Å]
1	−1953.30907	–	
2a	−4920.96862	0.0	11.77, 25.86
2b	−4920.94771	13.12	8.26, 18.65
3a	−4920.96104	0.0	6.53, 22.35
3b	−4920.94379	10.82	5.42, 20.66

10.82 kcal mol^{-1} (Table 1). Moreover, it has been found that in the *trans* form, both distamycin arms adopt a crescent shape and the pyrrole amide bonds orient opposite to each other around the azobenzene core. Isomerization brings both distamycin arms in close proximity. Therefore, the effective angle between two distamycin arms around the azobenzene core changes during photoisomerization, however, the extent of closeness between the distamycin arms in *cis* form of the ligands is very much dependent on the position of connectivity of the distamycin arms around the azobenzene core.

Synthesis

Compound **1** has been synthesized by adapting a procedure described earlier.[18] The synthesis of **2** started with the alkylation of 4,4′-dihydroxyazobenzene, **4** with greater than three equivalents of methyl bromoacetate in dry acetone under reflux conditions. The dimethyl ester, **5** was first hydrolyzed to the diacid, **6** and then converted to the corresponding acid chloride, **7**. This was then directly coupled with four equivalents of **1** in dry THF in the presence of *N*,*N*-diisopropylethylamine (DIEA) at room temperature to furnish **2** as an orange solid in approximately 50% yield of the isolated product after chromatographic purification over neutral alumina (Scheme 2).

Compound **3** was synthesized via 2,2′-dihydroxyazobenzene **8**, which was subjected to alkylation at both ends using more than three equivalents of methyl bromoacetate in dry acetone under reflux conditions. The dimethyl ester **9** was first hydrolyzed and then converted to the corresponding *N*-hydroxysuccinimide ester **11** by using 1,3-dicyclohexylcarbodiimide (DCC) in dry *N*,*N*-dimethylformamide (DMF). Finally, the activated diester **11** was coupled with excess **1** in THF at room temperature to afford **3** in 50% yield of the isolated product (Scheme 3). All final products and intermediates were fully characterized to ascertain their given structures.

Isomerization of the Conjugates in Solution

Azobenzene is photoactive and assumes one of two isomeric states (*cis* or *trans*) depending upon the wavelength of light used to illuminate the molecule. The *trans* isomer absorbs UV light at approximately 360 nm and upon illumination, it isomerizes into the *cis* isomer. Because the *cis* isomer absorbs light with a wavelength of 460 nm, illumination of the *cis* state with visible light causes the *cis* isomer to relax back to the *trans* isomer. As the absorption peaks of the two isomers overlap, complete conversion to the *cis* or *trans* isomer cannot generally be accomplished. Upon illumination, these systems therefore reach photostationary states that are comprised of a mixed population of *trans* and *cis* isomers. Thus, a detailed investigation of the isomerization process of the azobenzene in **2** and **3** (Scheme 1) is important to know the composition of the *trans* and *cis* isomeric forms at a photostationary state and to determine the kinetics of the *cis* to *trans* thermal-isomerization process in solution.

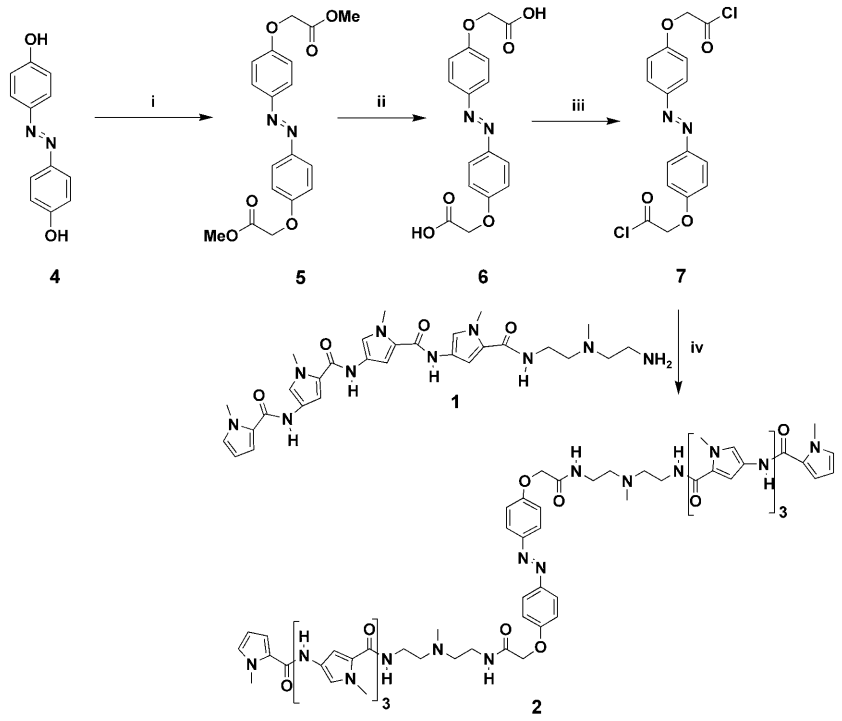

Scheme 2. Reagents, conditions, and yields. i) Methyl bromoacetate, K_2CO_3, [18]crown-6, acetone, reflux, 14 h, 75%; ii) 0.5 M NaOH, THF, reflux, 2 h, followed by acidification with 0.5 M HCl, 90%; iii) $SOCl_2$, THF, reflux, 3 h, 90%; iv) DIEA, THF, RT, 4 h, 50%.

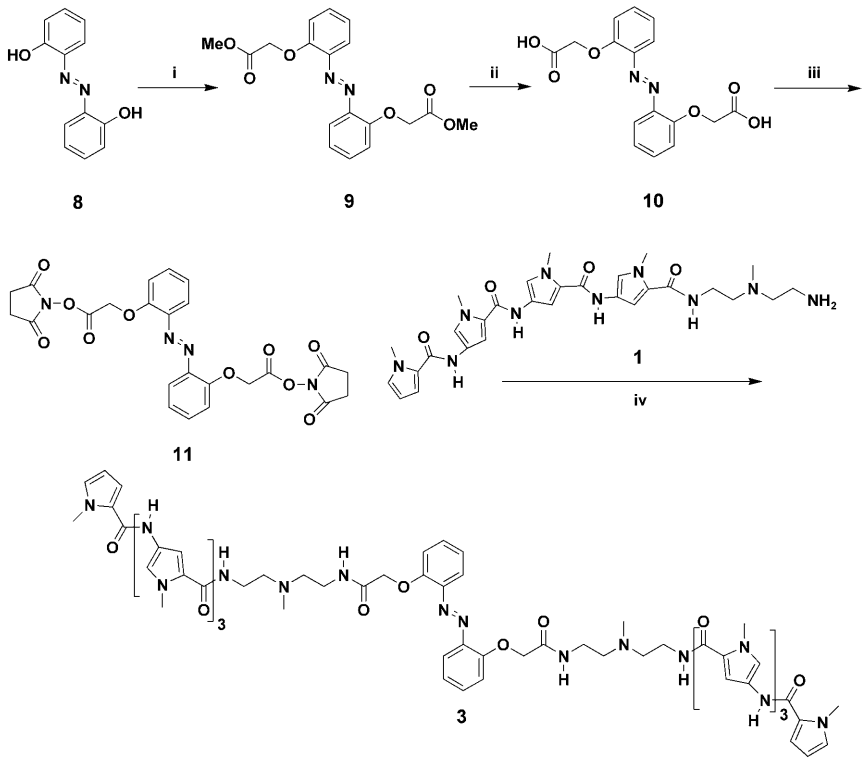

Scheme 3. Reagents, conditions, and yields. i) Methyl bromoacetate, K_2CO_3, [18]crown-6, acetone, reflux, 14 h, 70%; ii) 0.5 M NaOH, THF, reflux, 2 h, followed by acidification with 0.5 M HCl, 90%; iii) DCC, NHS, DMF, 0 °C, 30 min, then RT, 4 h, 99%; iv) THF, RT, 4 h, 50%. NHS = N-hydroxysuccinimide.

UV/Vis Spectral Study

The isomerization process was examined by irradiating the distamycin-based azobenzene conjugates **2** and **3** in DMSO solution at approximately 360 nm (Figure 1). Upon photoillumination of a solution of **2** (12 μM), the absorption band intensity at approximately 365 nm owing to the π–π* transition decreased with a considerable blue shift and the n–π* transition at approximately 450 nm increased. This process was continued over a period of 60 s and a photostationary state was reached. Similarly, illumination of a 24 μM DMSO solution of **3** for 60 s reduced the intensity of the π–π* transition and slightly reduced the magnitude of the n–π* transition. It required approximately 2 min to reach the photostationary state. No change was, however, observed at approximately 304 nm (distamycin band) for both the conjugates **2** and **3** upon photoillumination. These results indicate that *trans*-to-*cis* photoisomerization results in greater steric strain between the oligopeptide arms and azobenzene core in the *ortho–ortho* disubstituted azobenzene–distamycin conjugate **3** compared with its *para* disubstituted counterpart, **2**. This could be one of the reasons why a longer time was required for **3** compared with that of **2** to reach the photostationary state.

^{1}H NMR Spectral Study

^{1}H NMR spectroscopy provides a convenient way to determine the *cis* and *trans* composition of the ligands at the photostationary state. Accordingly, we monitored the changes in the ^{1}H NMR spectra of a solution (1 mM each) of **2** and **3** in [D_6]DMSO upon photoillumination at approximately 360 nm at periodic time intervals after each illumination. The results are shown in Figure 2 and Figure 3.

The ^{1}H NMR spectrum looked simpler for the conjugate **2** owing to the 4,4′-disubstituted symmetrical nature around the azobenzene core. Compound **2** in the *trans* isomeric state possessed hydrogen atoms in the 3, 3′, 5, and 5′ positions (*meta* protons to azo-

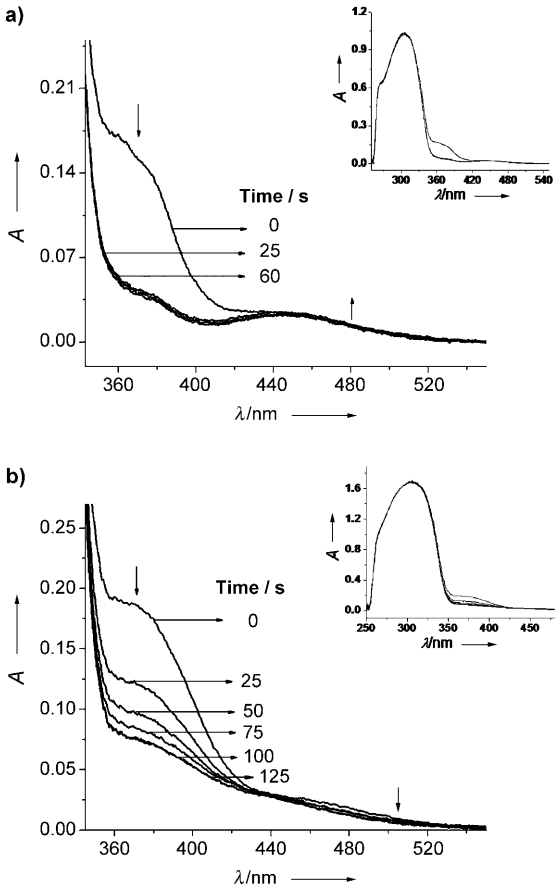

Figure 1. Changes in the absorption spectra of solutions of **2** (12 μM, a) and **3** (24 μM, b) in DMSO upon photoillumination at ~360 nm.

CHEMISTRY
AN ASIAN JOURNAL

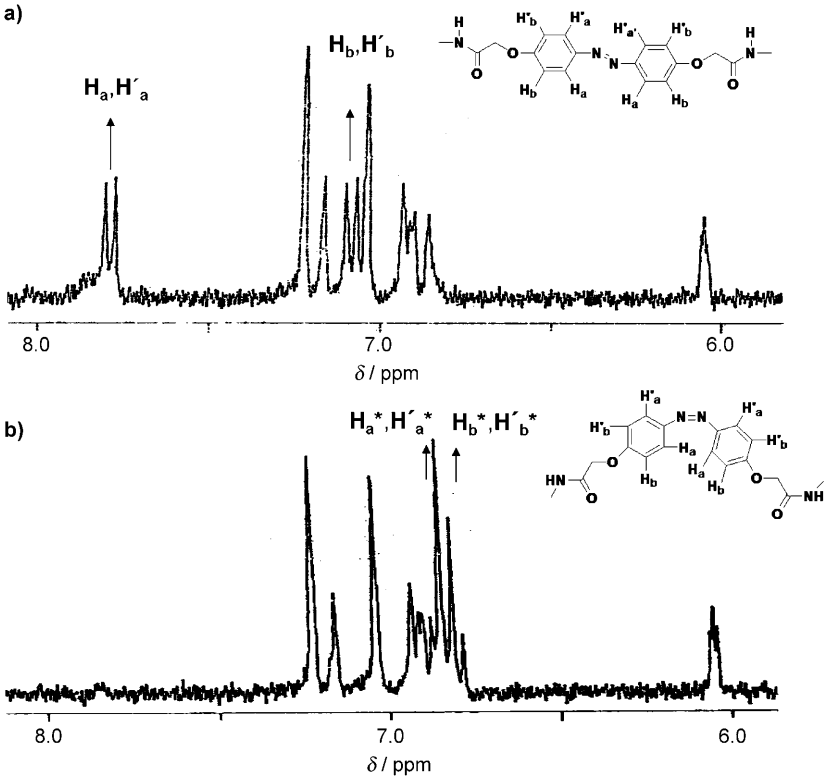

Figure 2. ^{1}H NMR spectra of a DMSO solution of 1 mM **2** before (a) and after (b) 10 min of photoillumination at ~360 nm. Chemical shifts of the respective azobenzene protons before and after illumination are indicated with respect to TMS as the standard. The symbol "*" refers to the sample after photoillumination.

benzene) at approximately 7.1 ppm ($J=8.7$ Hz), whereas the 2, 2′, 6, and 6′ hydrogen atoms (*ortho* protons to azobenzene) were positioned downfield (owing to the ring-current effect of the azobenzene ring) at approximately 7.8 ppm ($J=8.7$ Hz) at 25 °C (Figure 2a). Illumination of **2** for approximately 10 min completely shifted the 3, 3′, 5, and 5′ hydrogen atoms and the 2, 2′, 6, and 6′ hydrogen atoms upfield at approximately 6.8 and 6.86 ppm ($J=8.7$ Hz), respectively (Figure 2B). This interpretation of the spectrum is consistent with earlier observations.[19] Based on the NMR spectral study, approximately 10 min was required to reach the photostationary state for compound **2** in which approximately 100% of the *cis* isomeric form was generated in the photostationary state.

The azobenzene core in **3** possessed three different types of protons in the *trans* isomeric form. Both the *ortho* and *para* protons of the azobenzene (6, 6′, 4, 4′ hydrogen atoms) appeared like doublets at approximately 7.5 ppm ($J=$ 8.1 Hz) and a triplet at approximately 7.47 ppm ($J=8.7$ Hz), respectively (Figure 3a). The *meta* protons corresponding to 3, 3′, 5, 5′ hydrogen atoms appeared as multiplets at approximately 7.1–7.2 ppm. In addition to these, another set of peaks (less intense doublet-like and triplet-like peaks) appeared at approximately 6.6 ppm and 6.8 ppm, respectively. These peaks originated owing to the presence of a small amount (~20%) of the *cis* isomer of **3** at 25 °C. Although illumination of **3** for approximately 3 min intensified both peaks at approximately 6.6 and 6.8 ppm with $J=7.8$ Hz, within approximately 25 min, both downfield peaks at approximately 7.47 and 7.5 ppm shifted entirely upfield, maintaining the doublet and triplet multiplicity characteristics. At the same time, some proportion of the multiplet peaks corresponding to 3, 3′, 5, 5′ hydrogen atoms of the azobenzene moiety shifted upfield toward 6.85–6.9 ppm during isomerization. In spite of the changes in the azobenzene ring protons, only small changes were observed with the methylene hydrogen atoms connected with the 2, 2′ hydroxy groups of the azobenzene unit (Figure 3c). Such -CH_2- protons existed as two sharp singlets at 25 °C, as an intense singlet at approximately 4.7 ppm, and as a weak singlet at approximately 4.4 ppm. In the photostationary state, they were transformed into one intense singlet at approximately 4.4 ppm, with a weak singlet at approximately 4.7 ppm. Compound **3** required approximately 25 min to reach the photostationary state. Analysis of integration revealed that the composition of the two isomers *trans*/*cis* owing to **3** was approximately 8:2 at 25 °C before photoillumination. However, the relative composition of the isomers *trans*/*cis* transformed into approximately 2:8 in the photostationary state, which correlates well with earlier reports.[20]

Kinetics of *cis*-to-*trans* Isomerization and Thermal-Activation Parameters

To check the thermal reversibility of the photoisomerization process, the photoirradiated forms of both compounds **2** and **3** in solution were heated at different temperatures in the dark. Then, the kinetics of the thermal reversion of the conjugates from the *cis*-to-*trans* form was measured by following the changes in absorbance at a wavelength of 360 nm for the *para*- and 365 nm for the *ortho*-substituted azobenzene–distamycin conjugates. Expectedly, the thermal reversion process was found to be faster with the *para*-substituted azobenzene–distamycin conjugate **2** compared with the *ortho*-substituted conjugate **3**. A plot of log $[a_0/(a_0-a_t)]$ against time (t) afforded a straight line (correlation coefficient = 0.999, Figure 4a) indicating that the *cis*-to-*trans* thermal isomerization process of both **2** and **3** followed a first-order kinetic pathway. From the slope of the straight lines, the rate

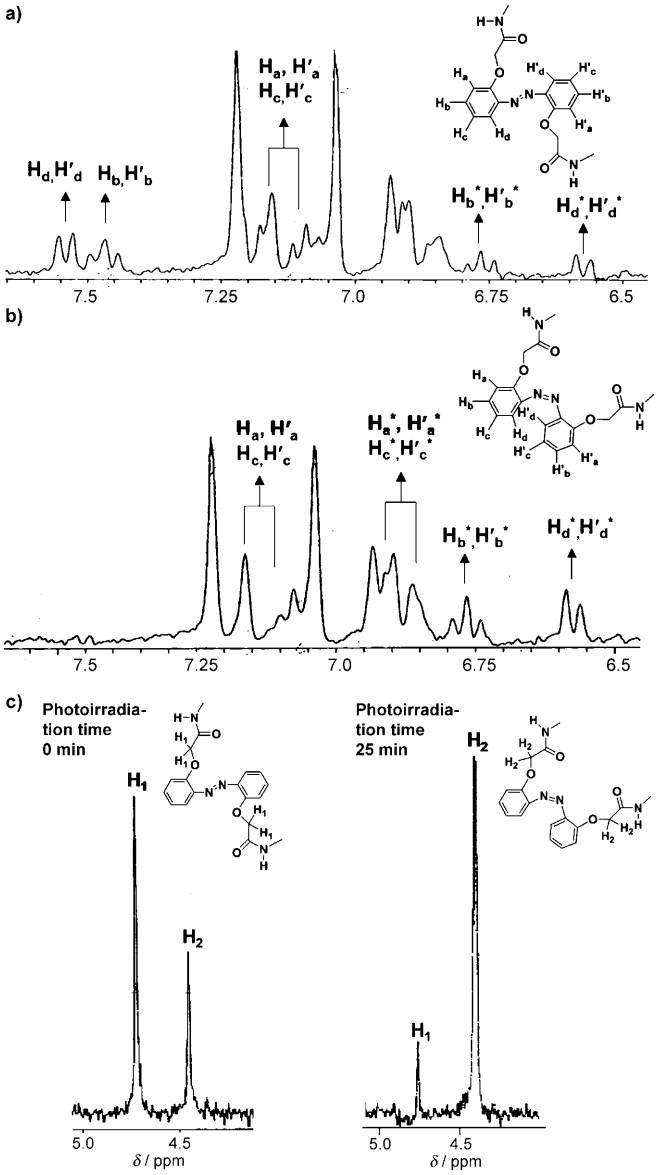

Figure 3. ^{1}H NMR spectra of a DMSO solution of 1 mM **3** before (a) and after (b) 25 min of photoillumination at ~360 nm. c) Chemical shifts of the $-OCH_2$ group before and after 25 min of photoillumination. Chemical shifts of the respective azobenzene protons and methylene protons before and after illumination are indicated with respect to TMS as standard. The symbol "*" refers to the sample obtained after photoillumination.

constants at different temperatures were obtained and the relevant values are given in Table 2. These rate constants at different temperatures also allowed us to calculate the activation energy (E_a) and the frequency factor (A) for the *cis*-to-*trans* thermal isomerization process by using the Arrhenius rate equation (Figure 4b). Both E_a and A were further used in the Eyring equation[19] to calculate the free energy ($\Delta G^{\neq}$), enthalpy ($\Delta H^{\neq}$), and entropy ($\Delta S^{\neq}$) of activation for the *cis*-to-*trans* isomerization of **2** and **3**. The relevant parameters are recorded in Table 3.

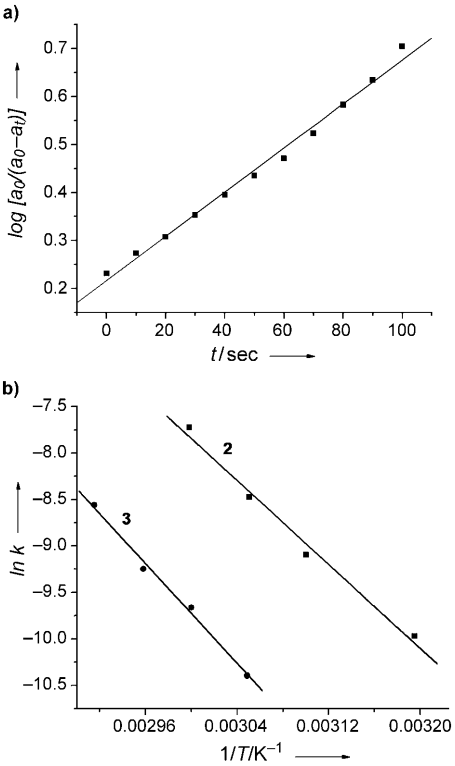

Figure 4. a) Plot of log $[a_0/(a_0-a_t)]$ versus time, t/sec, during the course of the thermal reversion of conjugate **3** at 60 °C. b) Arrhenius plots of the rate constant (k) for *cis*-to-*trans* thermal isomerization of **2** and **3** in DMSO followed at different temperatures (T).

Table 2. The rate constants of the *cis*-to-*trans* thermal isomerization of the azobenzene moiety of **2** and **3** in DMSO as monitored by UV/Vis spectroscopy.

Ligand	k[a] (40 °C) [s^{-1}]	k (50 °C) [s^{-1}]	k (55 °C) [s^{-1}]	k (60 °C) [s^{-1}]	k (65 °C) [s^{-1}]	k (70 °C) [s^{-1}]
2	4.7×10^{-5}	1.12×10^{-4}	2.1×10^{-4}	4.4×10^{-4}		
3			3.1×10^{-5}	6.4×10^{-5}	9.6×10^{-5}	19.1×10^{-5}

[a] The rate constant (k) of *cis*-to-*trans* thermal reversion was obtained by using the following equation, $\log[a_0/(a_0-a_t)]=k/2.303$, where a_0 = absorbance of ligand at room temperature before illumination, a_t = absorbance after heating the ligand solution at a particular temperature for time (t). See the Experimental Section for details.

Table 3. The activation energy, frequency factor, activation free energy, enthalpy, and activation entropy for thermal *cis*-to-*trans* isomerization of **2** and **3**.

Ligand	E_a[a] [kcal mol^{-1}]	A[a] [sec^{-1}]	$\Delta H^{\neq}$[b] [kcal mol^{-1}]	$\Delta S^{\neq}$[b] [kcal mol^{-1} K^{-1}]	$\Delta G^{\neq}$[b] [kcal mol^{-1}]
2	22.4	2.1×10^{11}	21.8	−4.5	23.2
3	26.5	1.6×10^{13}	25.9	−0.34	26.0

[a] Plot of rate constant vs temperature produces a straight line where the intercept and slope of the straight line determines the frequency factor (A) and activation energy (E_a), respectively, by using equation $\ln k=\ln A-E_a/RT$. [b] Free energy ($\Delta G^{\neq}$), enthalpy ($\Delta H^{\neq}$), and entropy ($\Delta S^{\neq}$) of activation were measured at 55 °C (328 K) by using the Eyring equation, where $E_a=\Delta H^{\neq}+RT$, and $\Delta S^{\neq}=[\ln A-1.00-\ln(k_BT/h)]R$, where k_B is the Boltzmann Constant and h is the Plank constant.

CHEMISTRY
AN ASIAN JOURNAL

These results indicate that both the molecular architecture and the location of the substituent around the core azobenzene moiety determine the rate and activation energy barrier for the *cis*-to-*trans* isomerization process. It has been found that once photoisomerized, the ligand **3** required a higher thermal-energy barrier to convert back to the *trans* form compared with that of ligand **2**. Such higher activation energy and frequency factor values for **3** indicate the larger structural change that occurs during *cis*-to-*trans* isomerization of **3** compared with **2**. Moreover, the larger frequency factor (*A*) for **3** was found to favor the *cis*-to-*trans* isomerization process entropically. However, the higher positive free energy of activation for the thermal isomerization of **3** compared with **2** indicates a different molecular environment of **3** in the *cis* configuration, which might impede the thermal *cis*-to-*trans* isomerization process.

Duplex-DNA Binding

CD Titration Studies with Poly [d(AT)]·poly [d(TA)]

It is of interest to study the variation in DNA-binding mode of two distamycin arms around the azobenzene core while changing the location of distamycins from 4,4′ to 2,2′ with respect to the azobenzene. To compare the DNA-binding affinity between the *trans* and *cis* isomeric forms of **2** and **3**, we carried out DNA-binding experiments separately with **2** and **3** before and after photoillumination by adding an aliquot of ligand solution into 20 μM poly [d(AT)]·poly [d(TA)] as shown in Figure 5 and Figure 6. Titration of compound **2** (*trans* form) at room temperature with poly [d(AT)]·poly [d(TA)] in NaCl buffer solution yielded negative and positive CD bands centered at 303 and 336 nm. These bands arose solely from the induction of optical activity of the DNA-bound non-chiral distamycin–azobenzene conjugate molecule (so-called induced CD).[21] The CD titration was also performed with compound **3** and its photoirradiated forms (Figure 6). Moderate ICD enhancement at 336 nm was observed with the 2:8 *trans*/*cis* isomeric form of **3** compared with that with the 8:2 *trans*/*cis* isomeric form. The saturation values of the [ligand]/[DNA] ([D]/[P]) ratios for individual isomeric forms of ligands (**2** and **3**) have been obtained by plotting ICD_{336} against [D]/[P] ratio. The azobenzene–distamycin conjugate **2**, in the *trans* form, required a [D]/[P] ratio of 0.3 and the corresponding *cis* isomer required a 0.2 [D]/[P] ratio to saturate its binding on the double-stranded DNA minor groove (Figure 7a). In contrast, the 8:2 *trans*/*cis* isomeric form of **3** required a [D]/[P] ratio of 0.46 and the corresponding value for the 2:8 *trans*/*cis* isomeric form is 0.4 (Figure 7b).

Trans-to-*cis* isomerization for both conjugates improved the duplex-DNA binding as evidenced from the lower [D]/[P] ratio to saturate DNA binding and higher ICD intensity compared with the corresponding *trans* forms. However, isomerization of **3** from the 8:2 *trans*/*cis* to the 2:8 *trans*/*cis* forms did not significantly improve the binding of its distamycin arms as reflected from the smaller difference in ICD values between isomeric forms of **3** obtained before and after photoisomerization. These observations suggest that the geometrical alignment of distamycin around the core azobenzene differ in both isomerized forms of **2** and **3**, which eventually causes the difference in their DNA-binding efficiencies. Thus, the overall difference in DNA recognition between both isomerized forms is not pronounced because the azobenzene isomerization here cannot bring both distamycin arms to an optimal orientation for the enhancement of the base-pair recognition along minor grooves while maintaining the duplex *B*-DNA structure.

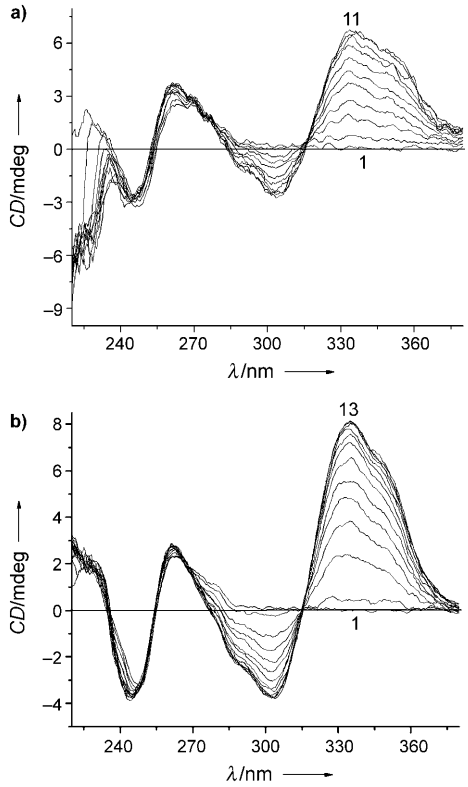

Figure 5. CD titration involving **2** in the 100% *trans* (a) and ~100% *cis* (b) form performed in presence of 20 μM poly [d(AT)]·poly [d(TA)] in 10 mM Tris-HCl, 150 mM NaCl, and 0.1 mM EDTA buffer solution at pH 7.4 and 25 °C under dark conditions. In panel (a) and (b), trace "1" corresponds to the CD spectrum of poly [d(AT)]·poly [d(TA)] and trace 11 and 13 correspond to the [conjugate]/[poly [d(AT)]·poly [d(TA)]] ratios of 0.4 and 0.3, respectively.

We also carried out DNA-binding experiments with the parent distamycin molecule **1** under the same experimental conditions to explain the binding mode and binding-site size of both isomeric forms of azobenzene–distamycin conjugates along the DNA minor groove. The ligand **1**, required a 0.2 [D]/[P] ratio to saturate DNA binding on the minor-groove surface (Figure 7c). This corresponds to an apparent binding-site sizes of approximately 5 base pairs, which correlates with the theoretical value expected for 2:1 overlapped binding mode.[21] The differences in DNA-binding mode between **1** compared with azobenzene–distamycin conjugates (**2** and **3**) have been explained in detail from theoretical perspectives (see below).

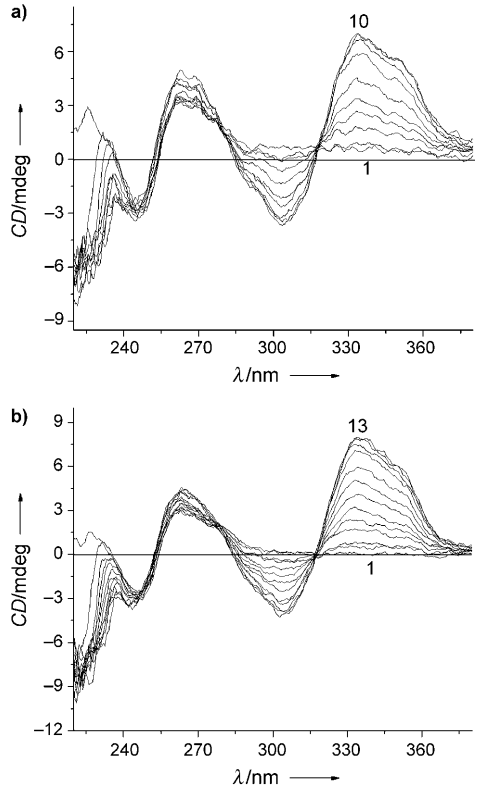

Figure 6. CD titration curves involving **3** in the 8:2 *trans*/*cis* (a) and 2:8 *cis*/*trans* (b) isomeric forms performed in presence of 20 μM poly [d(AT)]·poly [d(TA)] in 10 mM Tris-HCl, 150 mM NaCl, and 0.1 mM EDTA buffer solution at pH 7.4 and 25 °C under dark conditions. In panel (a) and (b), trace "1" corresponds to the CD spectrum of free poly [d(AT)]·poly [d(TA)] and trace 10 and 13 correspond to [ligand]/[poly [d(AT)]·poly [d(TA)]] ratio of 0.5.

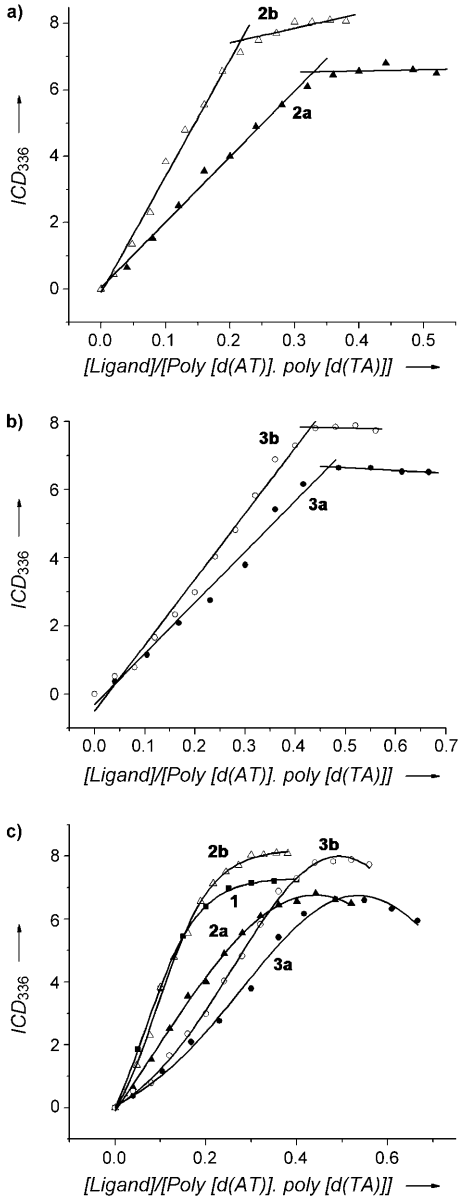

Figure 7. Comparison of the ICD intensities at 336 nm of both isomeric forms of ligands **2** (a) and **3** (b) obtained during titration with 20 μM poly [d(AT)]·poly [d(TA)] in NaCl buffer solution at 25 °C. **2a** and **2b** mentioned in the Figure correspond to the 100% *trans* and 100% *cis* form of the ligand **2**, whereas **3a** and **3b** correspond to the 8:2 *trans*/*cis* isomeric form and the 2:8 *trans*/*cis* isomeric form of the ligand **3**. c) Comparison of changes in 336 nm ICD intensities during titration with distamycin **1** and with both isomeric forms of ligands **2** and **3**, respectively, with 20 μM poly [d(AT)]·poly [d(TA)] in the same buffer solution at 25 °C.

Photoisomerization of DNA bound Conjugates

We also examined the influence of DNA binding on the photoisomerization of the DNA-bound ground state of the ligand by irradiating the sample at approximately 360 nm. This effect was examined by measuring the changes in the ICD band at 336 nm at 25 °C. Photoillumination of the *trans* form of ligand **2** (6 μM) bound to DNA (20 μM) for 10 min enhanced the ICD intensity at 336 nm. However, illumination for more than 10 min did not bring about any further change in the magnitude of the ICD band (Figure 8a). A similar experiment was also performed with the 2,2′-disubstituted azobenzene–distamycin conjugate, **3**. In this case, illumination of the sample for 30 min caused a small enhancement in ICD intensity, which did not change any further upon illumination of the sample beyond 30 min (Figure 8b). No change was observed in the DNA band, which confirmed that UV irradiation at 360 nm did not cause any significant changes in the poly [d(AT)]·poly [d(TA)] secondary structure.

Interestingly, for both ligands (**2** and **3**), there was an enhancement in the DNA binding after illumination of the DNA-bound *trans* forms. These observations suggest that the azobenzene group in **2** and **3** undergoes photoisomerization and enhances ICD intensity and hence their DNA-binding affinity even when the conjugate is complexed to the duplex-DNA minor groove. However, enhancement of such an ICD intensity is almost 50% less as compared with the ICD enhancement observed with the individual photoilluminated form of the ligands (**2** and **3**) than the corresponding *trans* form with a similar [D]/[P] value. Thus, the photoisomerization of the *trans*-to-*cis* form was suppressed when the ligand was pre-complexed to DNA.

CHEMISTRY
AN ASIAN JOURNAL

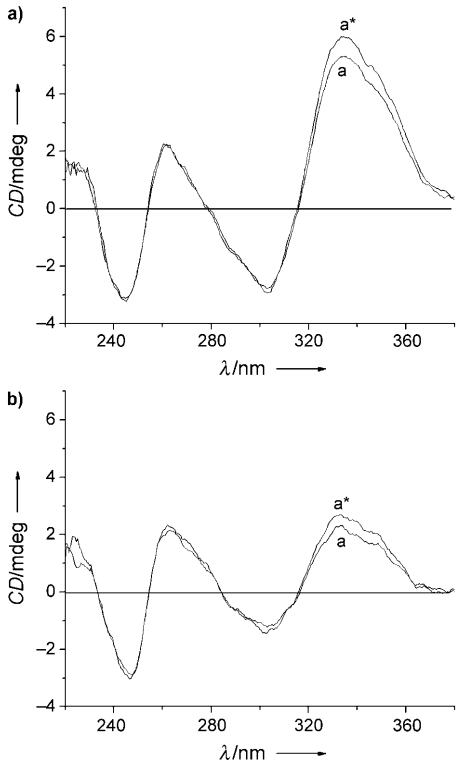

Figure 8. Changes in ICD intensity upon illumination at 360 nm of poly [d(AT)]·poly [d(TA)] precomplexed with ligand **2** or **3** at a [ligand]/[DNA] ratio of 0.3 in NaCl buffer solution. a) Trace a: ICD intensity of DNA bound to 100% *trans* form of ligand **2** and trace a* indicates the ICD intensity of the above ligand–DNA complex obtained after 10 min of photoillumination. b) ICD intensity of the DNA-bound approximate 8:2 *trans*/*cis* isomeric form of ligand **3**, and trace a* indicates the ICD intensity of the above ligand–DNA complex obtained after 30 min of photoillumination.

Duplex-DNA Melting Points

Minor-groove binders like distamycin and Hoechst 33258 enhance the helix-to-coil transition temperature through sequence-specific recognition of bases of duplex DNA.[15] Accordingly, we performed thermal-denaturation experiments with ligand–DNA complexes at a saturating [D]/[P] ratio in NaCl buffer solution. The DNA-melting experiment, as monitored by following the absorbance at 260 nm, demonstrates that the *trans* isomeric form of **2** and predominantly the *trans* (80%) isomeric form of ligand **3** stabilize duplex DNA more than that of the parent distamycin **1**. Compound **2** stabilized the duplex by approximately 9°C, whereas both isomeric forms of compound **3** stabilized poly [d(AT)]·poly [d(TA)] by approximately 13°C (Table 4). DNA complexed with both illuminated and non-illuminated solutions of ligands **2** and **3** possessed almost similar T_m values (Figure 9).

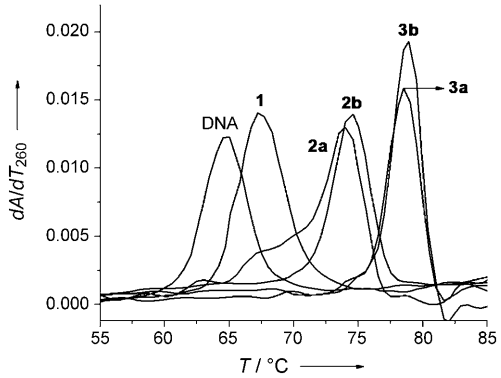

Figure 9. Thermal melting of 20 μM poly [d(AT)]·poly [d(TA)] complexed with various azobenzene–distamycin conjugates in 10 mM Tris-HCl, 150 mM NaCl, and 0.1 mM EDTA buffer solution at pH 7.4 and at saturating [ligand]/[DNA] ratios. The label of each curve corresponds to DNA: 20 μM poly [d(AT)]·poly [d(TA)] **1** at [D]/[P] = 0.2, **2a** and **2b** at [D]/[P] = 0.3, and 0.2, **3a** and **3b** at [D]/[P] = 0.46 and 0.4, respectively.

However, it is important to note that the photoilluminated forms of each ligand required a reduced concentration of ligand to reach the same T_m value as compared with the corresponding *trans* form, indicating greater thermal stabilization of duplex DNA by the *cis* forms of the conjugates.

Estimation of Binding Constants

Hoechst 33258 is a well-known DNA-minor-groove binder. The fluorescence emission owing to Hoechst dramatically enhances upon binding to duplex DNA.[22] We have experi-

Table 4. The melting temperatures values, apparent binding constants (K_{app}), and saturation [D]/[P] ratio obtained from binding of **1**, **2** and **3** in their ground state and upon photoillumination with poly [d(AT)]·poly [d(TA)] in NaCl buffer.[a]

Ligands	T_m [°C][b]	ΔT_m [°C][c]	K_{app}[d] [10^{-5} M^{-1}]	ΔG [kcal mol^{-1}]	Docked energy	*H*-bond distance[e] [Å]	Saturated [D]/[P]
1	67.4	2.7	6.5	−6.97	−11.29	2.50, 2.74, 2.32, 2.54	0.2
Hoechst				−12.1	−13.03	2.26, 2.18	
2a	74.5	9.8	7.4	−8.24	−21.93	3.35, 5.29, 6.54, 2.74, 4.61, 5.63	0.3
2b	74.0	9.3	7.2	−7.87	−21.57	3.49, 5.25, 5.78, 2.58, 2.92, 3.69, 4.85, 4.30, 2.56	0.2
3a	78.5	13.8	4.6	−8.63	−22.39	3.81, 4.54, 4.30, 3.03, 2.25, 2.67, 5.04, 5.51, 4.05	0.46
3b	78.9	14.2	4.8	−7.64	−21.33	3.97, 5.45, 5.46, 4.69, 3.50, 2.45, 4.27, 4.55, 3.52	0.4

[a] The docked energies, free binding energies (ΔG), and number of amide bond contacts with DNA bases obtained form Autodock calculations of different ligands with modeled duplex $[d(GC(AT)_{10}CG)]_2$ DNA are also tabulated. See the experimental section for details. [b] T_m indicates the average melting temperature value of two independent melting experiments that were preformed with the complexes of poly [d(AT)]·poly [d(TA)] in the presence of different ligands in 150 mM NaCl, 10 mM Tris-HCl, and 0.1 mM EDTA buffer solution, pH 7.4 at the saturated [D]/[P] ratio. The error is within ±0.2°C. [c] ΔT_m corresponds to the difference in T_m between DNA and DNA–ligand complexes. [d] K_{app} = apparent binding constant from Hoechst displacement assay. [e] Distance between the ligand, amide bond and DNA bases.

mentally determined the apparent DNA-binding constants of different isomeric forms of azobenzene–distamycin conjugates by estimating their efficiency in replacing fully bound Hoechst from the poly [d(AT)]·poly [d(TA)] DNA-minor-groove surface in NaCl buffer solution (Table 4).

Both isomeric forms of compounds **2** and **3** were added into saturated Hoechst–poly [d(AT)]·poly [d(TA)] complex solution. The *trans* form of **2** at room temperature was able to displace the DNA-bound Hoechst more efficiently than the *trans* isomeric form of **3**. This indicates a higher apparent binding constant for **2a** compared with **3a** at room temperature (Table 4). However, no significant changes in binding constant were observed between both isomeric forms of either **2** or **3.** This is a limitation of this indirect competitive binding assay unlike direct CD titration studies. Interestingly, both isomeric forms of **2** and **3** rapidly quench Hoechst fluorescence preferably when 50% of Hoechst was displaced from the duplex minor-groove surface (Figure 10). This fact

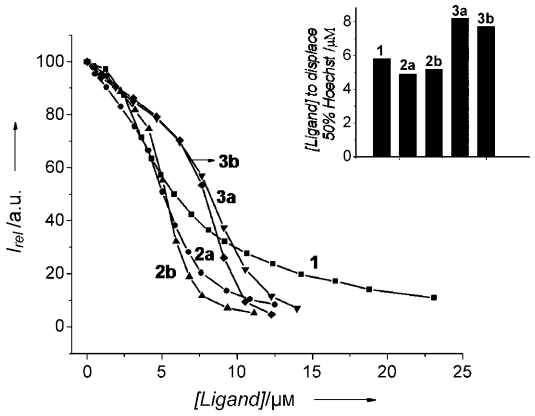

Figure 10. Changes in fluorescence intensity (I) of Hoechst while adding either distamycin analogue **1** or different photoisomeric forms of azobenzene–distamycin conjugates (**2a**, **2b**, **3a**, **3b**) into the saturated Hoechst–poly [d(AT)]·poly [d(TA)] complex in NaCl buffer solution at 25°C. Inset: y axis of the bar correspond to various ligand concentrations ($[L]_{50}$) to displace 50% Hoechst from the DNA minor-groove surface. Apparent binding constants (K_{app}) were calculated from the respective $[L]_{50}$ values and considering K_a (Hoechst) = 1.5×10^7 M^{-1} and [Hoechst 33258] = 250 nM.

clearly indicates the co-operative nature of ligand binding on the duplex minor-groove surface. Initial binding of the ligand might produce some conformational change on the DNA surface, which may allow preferred binding by the next ligand through concomitant removal of Hoechst from the duplex minor-groove DNA surface. Such a binding nature was found to be unique with azobenzene–distamycin covalent conjugates compared with the parent distamycin analogue.

Ligand Docking

To understand the experimental observations further, we explored the duplex-DNA binding of the ligands **1**–**3** by using the docking analysis with AUTODOCK version 3.05. The optimized distamycin analogue **1**, on rigid docking with $d[GC(AT)_{10}CG]_2$, gave a binding energy of −6.97 kcal mol^{-1} (Table 4) by satisfying four hydrogen bonding contacts between the *N*-methylpyrrole amide bond of the distamycin and the A–T base pairs of DNA and the other noncovalent interactions with the oxo group of the ribose sugar moiety (see Figure SI-1 in the Supporting Information). The number of hydrogen-bonding contacts support the DNA base-pair recognition efficiency of **1** as obtained from the saturation [D]/[P] ratio. The docking of **2a** shows that the azobenzene core allows both distamycin arms to satisfy the extended mode of binding unlike the hairpin conformation observed with the distamycin derivatives based on γ-amino butyric acid linkers.[23,24] More pyrrole amide bonds are available in the hydrogen-bonding contacts with AT base pairs, especially in the case of **2b** compared with **2a** as experimentally evidenced from the higher ICD intensity and lower [D]/[P] ratio of **2b** than **2a** (see Figure SI-1 in the Supporting Information and Table 4). In the *trans* form, either one or both benzene moieties of the planar azobenzene group is located close to the duplex-DNA surface to involve hydrophobic interactions with the DNA bases. Thus, in the presence of a long (~11 Å) linker unit, less pyrrole amides were able to form hydrogen-bonding contacts with the DNA bases. On the other hand, in the *cis* form, the nonplanar azobenzene moiety prefers to remain out of the DNA helical surface, which allows more pyrrole amide bonds to satisfy the hydrogen bonding interaction with the DNA bases. There is also another reason for the better hydrogen bonding contacts with the *para–para* disubstituted **2b** when compared with **2a**: an overall decrease in the length of the moiety $[-(CH_2)_2NMe(CH_2)_2NHXPhN{=}NPhXNH(CH_2)_2NMe(CH_2)_2-]$ (where X = $-OCH_2CO$) from 21.53 Å to 14.06 Å along with the linker that contains the azobenzene moiety together with a basic difference of approximately 3.5 Å around the azobenzene moiety [YPhN=NPhY] (where Y = O) during the *trans*-to-*cis* photoisomerization of **2** as obtained from the optimized conformation (see Figure SI-1 in the Supporting Information and Table 1).

This explains the improved ICD intensity of the *cis* form compared with the *trans* isomer. However, the difference in the saturated [D]/[P] ratio observed with these isomers cannot be explained by this argument. The difference in the orientation of **2b** and **2a** on the duplex-DNA surface was one of the factors that might contribute in the difference in the saturation [D]/[P] ratios. Moreover, the Hoechst displacement assay failed to show such a subtle difference in binding between **2b** and **2a** (7.2×10^{-5} M^{-1}, 7.4×10^{-5} M^{-1}) owing to the weaker contacts with the AT base pairs and the lower binding energy over Hoechst (−12.10 kcal mol^{-1}; Table 4). On the other hand, comparable thermal melting temperatures of **2a** and **2b** show that **2a** compensates its fewer number of hydrogen bonding contacts by a substantial stacking of the pyrrole units of distamycin arms and benzene units of azobenzene with the ribose sugar moiety along with the sum of van der Waals and electrostatic interactions with duplex DNA (see Figure SI-1 in the Supporting Infor-

mation). Hence, they have similar dock energies (−21.93, −21.57 kcal mol^{-1}) and binding energies (−8.24, −7.87 kcal mol^{-1}), much like the melting temperature values (Table 4). Such little difference in binding free energies between **2a** and **2b** supports the small variation in melting-temperature values and the apparent binding constant (K_{app}) values.

The docking conformation for the 2,2′-disubstituted ligands (**3a** and **3b**) also shows the extended binding mode (Figure SI-1 in the Supporting Information), however, both **3a** and **3b** show a similar range and number of hydrogen-bonding contacts with the AT base pairs. This is consistent with comparable ICD intensities between both isomeric forms of **3** (Table 4). This is because in the *ortho*-substituted azobenzene moiety there is a minimal variation in the length. This occurs with both isomers around the azobenzene moiety (~1.1 Å) or along the linker length containing the azobenzene moiety (from 22.35 Å to 20.66 Å) while transforming **3a** to **3b** (Table 4). The lower K_{app} (4.6×10^{-5} M^{-1} and 4.8×10^{-5} M^{-1}) obtained from experiments arises from the absence of strong hydrogen-bonding contacts with DNA bases and lower binding free energy compared with Hoechst. The gain of stacking, van der Waals, and electrostatic interactions are similar in both **3a** and **3b** owing to their minimal change in the length around the azobenzene core, which manifests in similar T_m values.

Conclusions

The azobenzene has been widely used as photoresponsive chromophore to regulate the molecular structure by *trans*-to-*cis* isomerization with light and its thermal reversion with heat. The incorporation of the azobenzene into the oligopeptide distamycin moiety provides a model system to probe the feasibility of this "light switch" in regulating DNA-binding characteristics through the introduction of a conformational change involving distamycin scaffolds. Herein, we report a convenient procedure to conjugate distamycin at different locations (2,2′ vs 4,4′) with respect to the core azobenzene unit. The detailed photoisomerization kinetics were examined by ^{1}H NMR and UV/Vis spectroscopy. The UV/Vis studies, kinetic analysis, and ^{1}H NMR spectroscopy indicate that photoisomerization depends on the location of the substituent around the azobenzene unit. Thus the *ortho–ortho* disubstituted ligand **3**, required longer for photoisomerization and also a higher thermal-energy barrier for *cis*-to-*trans* isomerization compared with that of ligand **2**.

The changes in DNA binding after photoisomerization were investigated by CD spectroscopy and thermal melting. The conformational freedom of distamycin was restricted while appended with the azobenzene core and this loss of flexibility was more pronounced with the *ortho–ortho* disubstituted conjugate **3** compared with its *para–para* counterpart **2**. This was reflected in the reduction in the ICD intensity, lower apparent binding constant, and requirement of higher ligand concentration to saturate the minor-groove binding by distamycin in ligand **3** compared with **2**. On the other hand, the requirement a reduced [ligand]/[DNA] ratio suggests that both isomeric forms of **2** favor distamycin binding along duplex DNA compared with that of **3**. The unique characteristics of both isomeric forms of azobenzene–distamycin conjugates, that is, the co-operative binding nature on the minor-groove surface of poly [d(AT)]·poly [d(TA)] and higher duplex-DNA stabilization of 7–11 °C more than their parent distamycin analogue **1**, are noteworthy. Work is now underway to examine the rate of photoisomerization and DNA-binding affinity of distamycin analogues by changing the electronic nature of the *para–para* disubstituted azobenzene core.[25]

Experimental Section

Materials and Methods

All reagents used in this study were of highest purity available and were used without further purification. TLC was performed by using silica gel-G and preparative column chromatography was done on silica gel (60–120 mesh size). Solvents such as CH_2Cl_2 and $CHCl_3$ were dried over P_2O_5, Et_3N was dried over KOH, THF was dried by using sodium and benzophenone ketyl, and DMF was vacuum distilled over anhydrous $MgSO_4$. ^{1}H NMR spectra were recorded on JEOL JNM λ-300 or with a Bruker AMX 400 spectrometer and ^{13}C NMR spectra were recorded on Bruker DMX 500 spectrometer. Chemical shifts (δ) are reported in ppm downfield from the internal standard (TMS). Electrospray ionization (ESI) mass spectra were measured on an Esquire spectrometer (Bruker). Compound **8** was commercially available and compound **4** was prepared as described earlier.[19] Distamycin analogue **1** is a tetra *N*-methylpyrrole-based tetrapeptide was synthesized as described.[13,18] Poly [d(AT)]·poly [d(TA)] is a double-stranded alternating copolymer and was obtained from Sigma Chem. Co. and used as received. Samples with total volume of 1 mL of poly [d(AT)]·poly [d(TA)] were prepared and 1 mg per ml of poly [d(AT)]·poly [d(TA)] afforded 20 A_{260} units. The concentration of poly [d(AT)]·poly [d(TA)] was determined spectrophotometrically by using $\varepsilon_{262}=6650$ M^{-1} DNA. The poly [d(AT)]·poly [d(TA)] concentration in the sample was 80 μM DNA phosphate (40 μM in terms of base pairs).

Photoisomerization and UV/Vis Analysis

Photoillumination was performed using a xenon lamp 450 with a light intensity of around 40 W, which transmitted light of approximately 360 nm. The photoisomerization was measured with a particular concentration of ligands **2** and **3** in DMSO by using a UV/Vis spectrophotometer (Shimadzu 2100) at 25 °C. The samples were irradiated at $\lambda\sim360$ nm and the time course of the photoisomerization process was monitored by recording the spectra at different time intervals. This provided the information on the time required for reaching a photostationary state of each azobenzene–oligopeptide conjugate. Once photostationary states were attained, each sample solution was then heated to a specific temperature and the corresponding spectral changes were recorded at that temperature after regular time intervals. A plot of log $[a_0/(a_0\text{-}a_t)]$ (where a_0 = absorbance of ligand at room temperature before illumination, a_t = absorbance after heating the ligand solution after illumination, at a particular temperature for time t) with time (t) furnished a straight line. This demonstrated that the photoisomerization of azobenzene in **2** and **3** followed first-order kinetics and the rate constant (k) could be obtained from the slope of the straight line. All kinetic experiments were carried out with a freshly prepared solution and each experiment was carried out at least twice. The observed k values were within ±3% of the value reported in Table 2.

The experimentally determined rate constants at different temperatures were plotted against $1/T$ (T = absolute temperature) to obtain the activation energy (E_a) and frequency factor (A) from the slope and intercept of the Arrhenius equation. Further, the activation enthalpies ($\Delta H^{\neq}$), activa-

tion entropies ($\Delta S^{\neq}$), and activation free energies ($\Delta G^{\neq}$) for the *cis*-to-*trans* isomerization of **2** and **3** were obtained from Eyring plots.[20,26]

^{1}H NMR Spectroscopy

^{1}H NMR experiments for the configurational analysis of conjugates **2** and **3** were carried out at 295 K by using a JEOL JNM λ-300 spectrometer. Individual samples of 1 mM concentration were taken in [D_6]DMSO and the corresponding changes in the molecular configuration upon photoillumination were determined by recording ^{1}H NMR spectra. Integration of the respective azobenzene proton peaks allowed the determination of the percentage of the *trans* and *cis* form of each ligands in their photostationary state.

Circular Dichroism Spectroscopy

CD spectra were recorded by using a JASCO (J-715) model spectropolarimeter equipped with a Perkin–Elmer temperature controller. The experiments were carried out in 150 mM NaCl, 0.01 M Tris-HCl (Tris = tris-(hydroxymethyl)aminomethane), 0.1 mM ethylenediaminetetracacetic acid (EDTA) buffer solution at pH 7.4 by using 20 μM duplex poly [d(AT)]·poly [d(TA)] in the presence and absence of the conjugates at 25 °C. All CD titrations were averaged over at least two acquisitions and the scan rate was maintained at 50 nm min^{-1} with optical cells of path length of 1 cm. Titration was performed in the dark and care was taken to minimize the isomerization of azobenzene–distamycin conjugates. The changes in ICD intensity at 336 nm were plotted against different [ligand]/[DNA] ratios to obtain the concentration of ligand required to saturate the duplex-DNA binding.

Effect on DNA Melting Points

The stabilities of ligand/duplex-DNA complexes were determined from thermal denaturation experiments. UV/Vis spectra were acquired on a Beckman 640 UV/Vis spectrophotometer equipped with a temperature programmable cell block by following the changes in absorbance at 260 nm as a function of temperature. The samples were heated at 0.5 °C min^{-1} and the absorbance values were recorded for every 0.5 °C rise in temperature. All T_m experiments were carried out twice in the above mentioned NaCl buffer solution at saturated [ligand]/[DNA] ratios. The average melting-temperature value of two independent melting experiments is mentioned in Table 4.

Hoechst Displacement Assay

The fluorescence intensity of Hoechst 33258 increases dramatically on binding with duplex poly [d(AT)]·poly [d(TA)]. Initially, 0.25 μM Hoechst was taken in NaCl buffer solution and various aliquots of concentrated poly [d(AT)]·poly [d(TA)] solution were added progressively to saturate Hoechst binding on the duplex-DNA surface. Different azobenzene–distamycin conjugates were then added into a saturated solution of Hoechst–DNA complex and the displacement of Hoechst from double-stranded DNA was measured by a decrease in the fluorescence emission intensity at 464 nm (λ_{ex} = 355 nm) and at 25 °C. Titration was performed under dark conditions and much care was taken to minimize the isomerization of azobenzene–distamycin hybrids. The concentration of individual ligands for achieving 50% quenching of DNA-bound Hoechst fluorescence was used for calculating the apparent binding constant (K_{app}). The binding constant (K_a) of Hoechst with poly [d(AT)]·poly [d(TA)] in NaCl buffer solution was found to be 1.5×10^7 M^{-1} by Scatchard analysis.[27]

Ligand-Docking Studies

A duplex oligodeoxynucleotide sequence of d[$GC(AT)_{10}CG]_2$ was presented to nucgen program of AMBER8[28] version instead of poly [d(AT)]·poly [d(TA)] DNA. The modeled duplex DNA was then docked with the optimized ligand structures by using AUTODOCK version 3.05.[29] The grid center was taken as a center of the macromolecule with a grid size of 80 × 80 × 126 and a grid spacing of 0.4186 Å. A Lamarckian genetic algorithm (GA) was used owing to the existence of 32–48 rotatable bonds in these ligands and to evaluate the right ligand–DNA conformation as it is known to reproduce various experimental ligand–DNA complex structures.[30] The flexible docking procedure was repeated until substantial interactions of the extended binding mode of the ligand with DNA were obtained. Further, the lowest dock conformation obtained from the flexible docking was again submitted for rigid docking to remove the internal energy of the ligand (steric clashes) by retaining the hydrogen-bonding interaction with the duplex-DNA bases.

Acknowledgements

We thank the Department of Biotechnology, Government of India for financial support of this work, Centre for Modeling, Simulation and Design (CMSD), and High Performance Computing Facility (HPCF), University of Hyderabad, Maui High Performance Computing Center (MHPCC) at Hawaii and the Supercomputer Education and Research Centre (SERC) of Indian Institute of Science for computational facilities. D.U.R. and S.D. acknowledge CSIR for senior research fellowships.

[1] H. Rau, *Photoisomerization of Azobenzene in Photochemistry and Photophysics*, *Vol. II*, CRC, Boca Raton, **1990**, p. 119.
[2] H. Rau in *Studies in Organic Chemistry, Photochroism, Molecules and Systems, Vol. 40* (Eds.: H. Dürr, H. Bouas-Laurent), Elsevier, Amsterdam, **1990**, p. 165.
[3] D. Liu, J. Karanicolas, C. Yu, Z. Zhang, G. Andrew Woolley, *Bioorg. Med. Chem. Lett.* **1997**, *7*, 2677.
[4] I. Willner, S. Rubin, *Angew. Chem.* **1996**, *108*, 419–439; *Angew. Chem. Int. Ed. Engl.* **1996**, *35*, 367–385.
[5] D. G. Flint, J. R. Kumita, O. S. Smart, G. A. Woolley, *Chem. Biol.* **2002**, *9*, 391–397.
[6] H. Asanuma, X. Liang, T. Yoshida, M. Komiyama, *ChemBioChem* **2001**, *2*, 39–44.
[7] X. Liang, H. Asanuma, M. Komiyama, *J. Am. Chem. Soc.* **2002**, *124*, 1877–1883.
[8] A. M. Caamano, M. E. Vazquez, J. Martinez-Costas, L. Castedo, J. L. Mascarenas, *Angew. Chem.* **2000**, *112*, 3234–3237; *Angew. Chem. Int. Ed.* **2000**, *39*, 3104–3107.
[9] L. Guerrero, O. S. Smart, C. J. Weston, D. C. Burns, G. A. Woolley, R. K. Allemann, *Angew. Chem.* **2005**, *117*, 7956–7960; *Angew. Chem. Int. Ed.* **2005**, *44*, 7778–7782.
[10] M. Liu, H. Asanuma, M. Komiyama, *J. Am. Chem. Soc.* **2006**, *128*, 1009–1015.
[11] L. A. Dickinson, R. J. Gulizia, J. W. Trauger, E. E. Baird, D. E. Mosier, J. M. Gottesfeld, P. B. Dervan, *Proc. Natl. Acad. Sci. USA* **1998**, *95*, 12890–12895.
[12] a) S. Bhattacharya, S. S. Mandal, *J. Chem. Soc. Chem. Commun.* **1995**, 2489–2490; b) S. Bhattacharya, S. S. Mandal, *Chem. Commun.* **1996**, 1515–1516; c) S. S. Mandal, N. V. Kumar, U. Varshney, S. Bhattacharya, *J. Inorg. Biochem.* **1996**, *63*, 265–272; d) S. S. Mandal, U. Varshney, S. Bhattacharya, *Bioconjugate Chem.* **1997**, *8*, 798–812.
[13] a) S. Bhattacharya, M. Thomas, *Biochem. Biophys. Res. Commun.* **2000**, *267*, 139–144; b) M. Thomas, U. Varshney, S. Bhattacharya, *Eur. J. Org. Chem.* **2002**, 3604–3615.
[14] S. Bhattacharya, M. Thomas, *Chem. Commun.* **2001**, 1464–1465.
[15] S. Ghosh, E. Defrancq, J. H. Lhomme, P. Dumy, S. Bhattacharya, *Bioconjugate Chem.* **2004**, *15*, 520–529.
[16] K. Seio, M. Mizuta, T. Terada, M. Sekine, *J. Org. Chem.* **2005**, *70*, 10311–10322.
[17] M. J. Frisch, G. W. Trucks, H. B. Schlegel, G. E. Scuseria, M. A. Robb, J. R. Cheeseman, J. A. Montgomery, Jr., T. Vreven, K. N. Kudin, J. C. Burant, J. M. Millam, S. S. Iyengar, J. Tomasi, V. Barone, B. Mennucci, M. Cossi, G. Scalmani, N. Rega, G. A. Petersson, H. Nakatsuji, M. Hada, M. Ehara, K. Toyota, R. Fukuda, J. Hasegawa, M. Ishida, T. Nakajima, Y. Honda, O. Kitao, H. Nakai, M. Klene, X. Li, J. E. Knox, H. P. Hratchian, J. B. Cross, C. Adamo, J. Jaramillo, R. Gomperts, R. E. Stratmann, O. Yazyev, A. J. Austin, R. Cammi, C. Pomelli, J. W. Ochterski, P. Y. Ayala, K. Morokuma, G. A. Voth, P. Salvador, J. J. Dannenberg, V. G. Zakrzewski, S. Dap-

prich, A. D. Daniels, M. C. Strain, O. Farkas, D. K. Malick, A. D. Rabuck, K. Raghavachari, J. B. Foresman, J. V. Ortiz, Q. Cui, A. G. Baboul, S. Clifford, J. Cioslowski, B. B. Stefanov, G. Liu, A. Liashenko, P. Piskorz, I. Komaromi, R. L. Martin, D. J. Fox, T. Keith, M. A. Al-Laham, C. Y. Peng, A. Nanayakkara, M. Challacombe, P. M. W. Gill, B. Johnson, W. Chen, M. W. Wong, C. Gonzalez, J. A. Pople, Gaussian 03 (Revision C.02), Gaussian, Inc., Wallingford CT, **2004**.

[18] S. Bhattacharya, M. Thomas, *Tetrahedron Lett.* **2000**, *41*, 5571–5575.

[19] W.-h. Wei, T. Tomohiro, M. Kodaka, H. Okuno, *J. Org. Chem.* **2000**, *65*, 8979–8987.

[20] A. Mamotake, T. Arai, *Tetrahedron Lett.* **2004**, *45*, 4131–4134.

[21] G. Luck, C. Zimmer, Karl-E Reinert, F. Arcamone, *Nucleic Acids Res.* **1977**, *4*, 2655–2670.

[22] F. G. Loontiens, P. Regenfuss, A. Zechel, L. Dumortier, R. M. Clegg, *Biochemistry* **1990**, *29*, 9029–9039.

[23] J. W. Trauger, E. E. Baird, P. B. Dervan, *J. Am. Chem. Soc.* **1998**, *120*, 3534–3535.

[24] C. R. Woods, T. Ishii, B. Wu, K. W. Bair, D. L. Boger, *J. Am. Chem. Soc.* **2002**, *124*, 2148–2152.

[25] S. Ghosh, D. Usharani, A. Paul, S. De, E. D. Jemmis, S. Bhattacharya, *Bioconjugate Chem.* in press.

[26] E. V. Brown, G. R. Granneman, *J. Am. Chem. Soc.* **1975**, *97*, 621–627.

[27] J. D. McGhee, P. H. von Hippel, *J. Mol. Biol.* **1974**, *86*, 469–489.

[28] Amber 8 version, Nicole A. T. F. et al. University of California, San Francisco.

[29] AutoDock 3.05; 10550 North Torrey Pines Road La Jolla CA 92037-1000 U. S. A.

[30] a) G. M. Morris, D. S. Goodsell, R. S. Halliday, R. Huey, W. E. Hart, R. K. Belew, A. J. Olson, *J. Comput. Chem.* **1998**, *19*, 1639–1662; b) D. A. Evans, S. Neidle, *J. Med. Chem.* **2006**, *49*, 4232–4238; c) C. Detering, G. Varani, *J. Med. Chem.* **2004**, *47*, 4188–4201; d) K. Chen, S. J. Adelstein, A. I. Kassis, *J. Mol. Struct. Theochem.* **2004**, *711*, 49–56.

Received: April 1, 2008
Published online: September 22, 2008

